Geomechanics and Engineering, *Vol. 32, No. 2 (2023) 145-157*
https://doi.org/10.12989/gae.2023.32.2.145

Face stability analysis of large-diameter underwater shield tunnel in soft-hard uneven strata under fluid-solid coupling

Shanglong Zhang[1], Xuansheng Cheng*[1,2], Xinhai Zhou[1] and Yue Sun[1]

[1]*Key Laboratory of Disaster Prevention and Mitigation in Civil Engineering of Gansu Province, Lanzhou University of Technology, No. 287, Langongping Road, Lanzhou 730050, China*
[2]*Western Engineering Research Center of Disaster Mitigation in Civil Engineering of Ministry of Education, Lanzhou University of Technology, No. 287, Langongping Road, Lanzhou 730050, China*

(*Received September 29, 2022, Revised November 8, 2022, Accepted December 24, 2022*)

Abstract. This paper aims at investigating the face stability of large-diameter underwater shield tunnels considering seepage in soft-hard uneven strata. Using the kinematic approach of limit upper-bound analysis, the analytical solution of limit supporting pressure on the tunnel face considering seepage was obtained based on a logarithmic spiral collapsed body in uneven strata. The stability analysis method of the excavation face with different soft- and hard-stratum ratios was explored and validated. Moreover, the effects of water level and burial depth on tunnel face stability were discussed. The results show the effect of seepage on the excavation face stability can be accounted as the seepage force on the excavation face and the seepage force of pore water in instability body. When the thickness ratio of hard soil layer within the excavation face exceeds 1/6*D*, the interface of the soft and hard soil layer can be placed at tunnel axis during stability analysis. The reliability of the analytical solution of the limit supporting pressure is validated by numerical method and literature methods. The increase of water level causes the instability of upper soft soil layer firstly due to the higher seepage force. With the rise of burial depth, the horizontal displacement of the upper soft soil decreases and the limit supporting pressure changes little because of soil arching effect.

Keywords: arching effect; face stability; limit analysis; numerical analysis; seepage; soil underwater tunnel; upper-soft and lower-hard strata

1. Introduction

When an underwater shield tunnel crossing river is excavated, the shield always passes through the soft-hard heterogeneous ground. Owing to the effects of stratum lithologic, and the high water pressure seepage, the tunneling direction is prone to deviation when the supporting pressure on the tunnel face is not appropriately controlled. Additionally, the front part of the shield equipment is heavy, and the tail is relatively light, which can easily lead to the bump of the shield machine. The above factors result in the tunneling posture being out of control, which seriously affects the ground settlement and the construction efficiency of the shield tunneling. Therefore, it is essential to conduct the face stability investigation of shield tunnel accounting high water level seepage in the soft-hard heterogeneous ground.

Researchers mainly employ the limit equilibrium analysis, the plastic limit analysis, the numerical method, and the model test approach to investigate of the tunnel face stability. Based on Horn's 3D wedge-silo model (1961), Anagnostou and Kovári (1996) established a three-dimensional wedge-prism model in the homogeneous stratum, and the limit supporting pressure of the shield tunnel face was studied using the limit equilibrium analysis. These years, scholars modified the wedge model (Broere 2001, Anagnostou 2012, Hu *et al.* 2012, Chen *et al.* 2019) and further explored the tunnel face stability taking the seepage effect into account (Perazzelli *et al.* 2014, Qiao *et al.* 2010). The calculation model of the limit equilibrium method is intuitionistic, and the theoretical calculation is relatively easy. However, the instability model does not follow the equations of solid mechanics well, and the motion tolerance condition of the instability body is also not considered. Based on the stability factor reported by Broms and Bennermark (1967), the lower-bound solution of the tunnel face stability factor for Tresca material was investigated by Davis *et al.* (1980) employing the limit analysis method. According to Davis's research, Leca and Dormieux (1990) presented the upper-bound methods for one and two conical sliding blocks, and investigated the excavation face stability for Mohr-Coulomb material. Later, researchers modified the conical instability models (Mollon *et al.* 2010, Mollon *et al.* 2011), and the analytical solutions of the limit supporting pressure with higher accuracy were obtained. In General, the theory of plastic limit analysis is more strict, and the solving process is relatively simple, and it has significant advantages in conducting the investigation of soil mechanical stability. For instance, employing the limit upper-bound analysis, the effect of nonhomogeneous soil layer (Ibrahim *et al.* 2015, Han *et al.* 2016, Zhong and Yang 2020, Wang *et al.* 2021) and pore water pressure (Lee *et al.* 2003, Wang *et al.* 2013, Zou and Qian 2018, Xue *et al.* 2019) on the tunnel face stability were studied by means

*Corresponding author, Professor
E-mail: chengxslut@sina.com

ISSN: 2005-307X (Print), 2092-6219 (Online)

of the optimized failure model.

Moreover, the numerical analysis method is an available method to deal with engineering issues because of its strong ability to perform mechanical analysis under complex multi-factor conditions. Scholars usually use the Finite Element Method (Ukritchon *et al.* 2017, Cheng *et al.* 2018, Alagha and Chapman 2019), the Finite Difference Method (Zhang *et al.* 2020, Cheng *et al.* 2021), and the Discrete Element Method (Chen *et al.* 2011, Hu and Zhang 2013, Lei *et al.* 2021) for the investigations of the face stability of tunnels. Ukritchon *et al.* (2017) studied the effects of the cover depth ratio, overburden stress factor, and linear strength gradient ratio on the load factor of the undrained tunnel face stability by three-dimensional finite element analysis. Zhang *et al.* (2020) investigated the face stability of a horseshoe-shaped shield tunnel in undrained clays with a linearly increasing strength by FLAC3D. Chen *et al.* (2011) explored the limit supporting pressure, failure zone and, soil arching of shallow shield tunnels in dry sandy ground by using the discrete element method. In addition, researchers (Idinger *et al.* 2011, Ahmed and Iskander 2012, Chen *et al.* 2013, Lv *et al.* 2016, Chen *et al.* 2018) studied the tunnel face stability under various geological conditions by using the model test method, and some substantial laws about the tunnel face stability are revealed.

Researchers have obtained a great many results in the investigation of tunnel face stability, and a large number of studies have been conducted on tunnel face stability in heterogeneous layers more recently (Tang *et al.* 2013, Senent and Jimenez 2015, Wang 2017, Lu *et al.* 2021). However, most researchers do not take into consideration the effect of groundwater seepage, or only the impact of pore water single seepage is accounted in some studies of the tunnel face stability, and the fluid-solid coupling effect is ignored. Additionally, the impact of high water pressure seepage, burial depth, and soil arching effect on the excavation face stability should be thoroughly analyzed for a large-diameter underwater tunnel crossing the soft-hard heterogeneous ground. Therefore, in this study, a logarithmic spiral collapsed model of a large-diameter underwater tunnel face was established in soft-hard heterogeneous strata, and the analytical solution of the limit supporting pressure accounting seepage was derived employing the limit upper-bound analysis method. The stability analysis method of excavation face with different soft- and hard-stratum ratios was determined, and the analytical solution of the limit supporting pressure was validated by numerical method and literature methods. In addition, the effect of water level and burial depth on the excavation face stability was further discussed.

2. Upper-bound solution of tunnel face stability in soft-hard uneven strata

2.1 Instability failure mode accounting seepage

The active instability mode of a large-diameter underwater tunnel face in homogeneous stratum (Zhang *et al.* 2022) was improved. An active instability mode of the tunnel face in soft-hard heterogeneous strata under seepage was established, as Fig. 1 shows. The water level over the riverbed was H, the tunnel burial depth was C, and the diameter of the tunnel was D. AB represented the tunnel excavation face, and the logarithmic spiral AF, BI and IF turned around the rotation center point O. The spirals started from the arch bottom point B, the terminal point I of BI spiral and the vault point A, respectively, and intersected at point F. The instability body $AFIB$ rotated around the point O at an invariable speed w. The lengths of OB, OI, OA, and OF are r_{OB}, r_{OI}, r_{OA} and r_{OF}, respectively, and the angles between OB, OI, OA, and OF and OV are θ_B, θ_I, θ_A, and θ_F, respectively. Within the excavation face, the thickness of the soft soil layer is $(1\text{-}n)D$, and the thickness of the hard soil layer is nD. n is the ratio of the thickness of the hard soil layer to the height of the excavation face.

The equations of logarithmic spiral AF, BI, and IF are

$$\mathrm{AF}: r_1 = r_1(\theta) = r_{OA}\ \exp\left[(\theta - \theta_A)\tan\varphi_1\right] \tag{1}$$

$$\mathrm{BI}: r_2 = r_2(\theta) = r_{OB}\ \exp\left[(\theta_B - \theta)\tan\varphi_2\right] \tag{2}$$

$$\mathrm{IF}: r_3 = r_3(\theta) = r_{OI}\ \exp\left[(\theta_I - \theta)\tan\varphi_1\right] \tag{3}$$

The geometrical relations in $\triangle OAB$ are

$$\frac{r_{OA}}{\sin\theta_B} = \frac{r_{OB}}{\sin OAB} = \frac{r_{OB}}{\sin\theta_A} \Rightarrow r_{OA} = \frac{r_{OB}\cdot\sin\theta_B}{\sin\theta_A} \tag{4}$$

$$r_{OB} = \frac{D\cdot\sin\theta_A}{\sin\left(\theta_A - \theta_B\right)} \tag{5}$$

Where, φ_1, and φ_2 are the internal friction angles of the upper soil and the lower soil, respectively.

$$r_{OI} = r_{OB}\cdot\exp\left[\left(\theta_B - \theta_I\right)\tan\varphi_2\right] \tag{6}$$

$$r_{OB}\cdot\cos\theta_B = H_0 + D \tag{7}$$

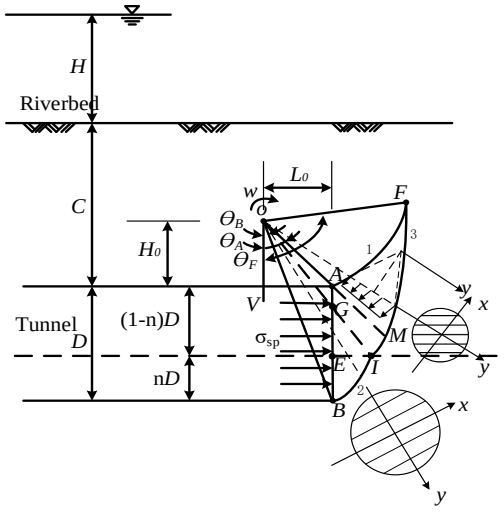

Fig. 1 Instability mode of underwater shield tunnel face

$$r_{OI}\cdot\cos\theta_I = H_0 + (1-n)D \tag{8}$$

From Eqs. (7) and (8)

$$r_{OB}\cdot\cos\theta_B - r_{OI}\cdot\cos\theta_I = nD \tag{9}$$

Substituting Eq. (6) into Eq. (9)

$$\cos\theta_B - \exp\left[(\theta_B-\theta_I)\tan\varphi_2\right]\cos\theta_I = \frac{n\cdot\sin(\theta_A-\theta_B)}{\sin\theta_A} \tag{10}$$

θ_I can be obtained from Eq. (10)

$$\begin{aligned} &r_{OF} = r_{OA}\ \exp\left[(\theta_F-\theta_A)\tan\varphi_1\right] = r_{OB} \\ &\exp\left[\theta_B\tan\varphi_2 - \theta_I(\tan\varphi_2-\tan\varphi_1) - \theta_F\tan\varphi_1\right] \end{aligned} \tag{11}$$

$$\begin{aligned} \theta_F = \frac{1}{2\tan\varphi_1}[&\theta_B\tan\varphi_2 + \theta_A\tan\varphi_1 \\ &-\theta_I(\tan\varphi_2-\tan\varphi_1) - \ln\frac{\sin\theta_B}{\sin\theta_A}] \end{aligned} \tag{12}$$

2.2 Power calculation

It is supposed that the soil obeys the Mohr-Coulomb yield criterion, the soil deformation submits to the small deformation hypothesis, and the displacement velocity field of the instability body in soil masses is kinematically admissible.

2.2.1 Exterior force power

The loads affecting the stability of the underwater shield tunnel face are considered as follows: (1) Supporting pressure on the excavation face σ_{sp}; (2) Soil self-weight σ_r; (3) Seepage force σ_u. The impact of pore water seepage on the tunnel face stability can be accounted as: ① The impact of the seepage force $\sigma_{u'}$ on the excavation surface. Taking average pore water pressure on the excavation surface as seepage force on it under steady seepage condition; ②The impact of the pore water seepage on the instability body.

(1) Supporting pressure power

The uniform supporting pressure acts on the tunnel face when the shield works.

$$\begin{aligned} W_{sp} &= \sigma_{sp}\int_L v_i n_i dL = \sigma_{sp}\int_L v_i\cos\theta dL \\ &= w\sigma_{sp}r_{OB}^2\sin^2\theta_B\int_{\theta_B}^{\theta_A}\frac{\cos\theta}{\sin^3\theta}d\theta \end{aligned} \tag{13}$$

(2) Power of soil self-weight

It is supposed that the instability body in the soft-hard heterogeneous strata consists of a number of circles, the circle radius in the soft soil layer is $R_1(\theta)$, and the circle center is $r_{m1}(\theta)$ from the point O, where $R_1(\theta)=\frac{r_3(\theta)-r_1(\theta)}{2}$, $r_{m1}(\theta)=\frac{r_3(\theta)+r_1(\theta)}{2}$. The radius of each circle in the hard soil layer is $R_2(\theta)$, and the circle center is $r_{m2}(\theta)$ from the point O, where $R_2(\theta)=\frac{r_2(\theta)-r_1(\theta)}{2}$, $r_{m2}(\theta)=\frac{r_2(\theta)+r_1(\theta)}{2}$.

Introducing three new variables, $a_1=\frac{r_{OB}\sin\theta_B}{\sin\theta}-r_{m1}$, $a_2=\frac{r_{OB}\sin\theta_B}{\sin\theta}-r_{m2}$ and $a_3=\frac{r_{OI}\cos\theta_I}{\cos\theta}-r_{m2}$, the instability body is divided into block 1 (*AFM*), block 2 (*AMIG*), block 3 (*GIE*), and block 4 (*EIB*), and then the self-weight power of the soil W_r is

$$W_r = W_{r1}+W_{r2}+W_{r3}+W_{r4} \tag{14}$$

$$\begin{aligned} W_{r1} &= wr_1\int_{\theta_A}^{\theta_F}\int_{-R_1}^{R_1}(r_{m1}+y)^2\sin\theta dyd\theta \\ &= 2wr_1\int_{\theta_A}^{\theta_F}\left(R_1r_{m1}^2+\frac{R_1^3}{3}\right)\sin\theta d\theta \end{aligned} \tag{15}$$

$$\begin{aligned} &W_{r2} = wr_1\int_{\theta_I}^{\theta_A}\int_{a_1}^{R_1}(r_{m1}+y)^2\sin\theta dyd\theta = wr_1\cdot \\ &\int_{\theta_I}^{\theta_A}\left(r_{m1}^2(R_1-a_1)+r_{m1}(R_1^2-a_1^2)+\frac{R_1^3-a_1^3}{3}\right)\sin\theta d\theta \end{aligned} \tag{16}$$

$$\begin{aligned} &W_{r3} = wr_1\int_{\theta_B}^{\theta_I}\int_{a_2}^{R_2}(r_{m2}+y)^2\sin\theta dyd\theta = wr_1\cdot \\ &\int_{\theta_B}^{\theta_I}\left(r_{m2}^2(R_2-a_2)+r_{m2}(R_2^2-a_2^2)+\frac{R_2^3-a_2^3}{3}\right)\sin\theta d\theta \end{aligned} \tag{17}$$

$$\begin{aligned} W_{r4} &= w(r_2-r_1)\int_{\theta_B}^{\theta_E}\int_{a_2}^{R_2}(r_{m2}+y)^2\sin\theta dyd\theta \\ &+w(r_2-r_1)\int_{\theta_E}^{\theta_I}\int_{a_3}^{R_2}(r_{m2}+y)^2\sin\theta dyd\theta \end{aligned} \tag{18}$$

(3) Seepage force power

① The seepage force power on the excavation surface

$$W_{u'} = w\sigma_u r_{OB}^2\sin^2\theta_B\int_{\theta_B}^{\theta_A}\frac{\cos\theta}{\sin^3\theta}d\theta \tag{19}$$

② The power of pore water seepage in the instability body

When the seepage reaches a steady state, the tunnel face stability is considered to be affected by the horizontal hydraulic gradient before the excavation face, and the vertical hydraulic gradient over the tunnel. To make the issue easy to calculate, the instability body *AFIB* is partitioned into block *AFM*, block *AMIG* and block *GIB*, as Fig. 1 shows. In block *AFM*, the impact of the vertical seepage force is mainly accounted, and the impact of the horizontal seepage force is primarily taken into account in block *AMIG* and block *GIB*.

It is assumed that the water head height at the surface of riverbed is h, and the water head height around the excavation face is h_0. Therefore, the vertical hydraulic gradient in the soil over the tunnel is

$$i_v = \frac{h-h_0}{C} \tag{20}$$

The power of the vertical seepage force in block AFM is

$$\begin{aligned} W_{u1} &= \int_{S_{AFM}} r_w\vec{i}ds_j v_j\sin\theta \\ &= 2wr_w\frac{h-h_0}{C}\int_{\theta_A}^{\theta_F}\left(R_1r_{m1}^2+\frac{R_1^3}{3}\right)\sin\theta d\theta \end{aligned} \tag{21}$$

Table 1 Property parameters of the stratum

	Natural weight (N/m^3)	E (Pa)	μ	φ (°)	c (Pa)	Permeability coefficient (m/s)
Muddy clay	17.5×10^3	10×10^6	0.3	20	14×10^3	1×10^{-8}
Limestone soil	23.4×10^3	20×10^7	0.21	40	20×10^3	1×10^{-10}

In the soft-hard heterogeneous strata, the permeability coefficient of the upper soil layer is K_1, and the permeability coefficient of the lower soil layer is K_2. The average permeability coefficient of the soil the shield passes through is

$$K_3=\frac{D}{\frac{(1-n)D}{K_1}+\frac{nD}{K_2}}=\frac{K_1K_2}{K_2(1-n)+K_1n} \tag{22}$$

The flow differential equation of the crossing soil layer is

$$K_3\frac{\partial^2 H}{\partial z^2}+\frac{K_1}{C}\cdot\frac{\partial H}{\partial z}=0 \tag{23}$$

The constraint conditions for the above equation are

$$\begin{cases} z=0, & H=h_0 \\ z=c, & H=h \end{cases} \tag{24}$$

The horizontal hydraulic gradient before the tunnel excavation face is

$$\begin{aligned} i_h&=\frac{\partial H}{\partial x}=\frac{h-h_0}{e^{-\frac{K_1}{K_3}}-1}e^{-\frac{K_1}{CK_3}z}\left(-\frac{K_1}{CK_3}\right)\\ &=\frac{(h-h_0)\left(-\frac{K_2(1-n)+K_1n}{CK_2}\right)}{e^{-\frac{K_2(1-n)+K_1n}{K_2}}-1}e^{-\frac{K_2(1-n)+K_1n}{CK_2}z} \end{aligned} \tag{25}$$

Horizontal seepage force power in the AMIB block is

$$\begin{aligned} W_{u2}&=\int_{S_{\Delta ABB}} r_w\vec{i}ds_j v_j\cos\theta=wr_w i_h|_{z=1}[\int_{\theta_I}^{\theta_A}\int_{a_1}^{R_1}(r_{m1}+y)^2\cos\theta dyd\theta+\int_{\theta_B}^{\theta_I}\int_{a_2}^{R_2}(r_{m2}+y)^2\cos\theta dyd\theta]\\ &=wr_w\frac{(h-h_0)(-\frac{K_2(1-n)+K_1n}{CK_2})}{e^{-\frac{K_2(1-n)+K_1n}{K_2}}-1}e^{-\frac{K_2(1-n)+K_1n}{CK_2}}\{\int_{\theta_I}^{\theta_A}(r_{m1}^2(R_1-a_1)+r_{m1}(R_1^2-a_1^2)+\frac{R_1^3-a_1^3}{3})\cos\theta d\theta+\\ &\int_{\theta_B}^{\theta_I}(r_{m2}^2(R_2-a_2)+r_{m2}(R_2^2-a_2^2)+\frac{R_2^3-a_2^3}{3})\cos\theta d\theta\} \end{aligned} \tag{26}$$

The seepage force power in the instability body *AFIB* is

$$W_u=W_{u'}+W_{u1}+W_{u2} \tag{27}$$

2.2.2 Interior energy dissipation

The interior energy dissipation of the instability body *AFIB* is accounted to take place on the surfaces of *AF*, *BI*, and *IF*, and the energy dissipation on the surface *AF*, *BI*, and *IF* are calculated as follows

$$\begin{aligned} D_{AF}&=\int_{\theta_A}^{\theta_F}c_1wr_1^2(\theta)d\theta\\ &=\frac{c_1wr_{OA}^2}{2\tan\varphi_1}\left\{\exp\left[2(\theta_F-\theta_A)\tan\varphi_1\right]-1\right\} \end{aligned} \tag{28}$$

$$\begin{aligned} D_{BI}&=\int_{\theta_B}^{\theta_I}c_2wr_2^2(\theta)d\theta\\ &=\frac{c_2wr_{OB}^2}{2\tan\varphi_2}\left\{-\exp\left[2(\theta_B-\theta_I)\tan\varphi_2\right]+1\right\} \end{aligned} \tag{29}$$

$$\begin{aligned} D_{IF}&=\int_{\theta_I}^{\theta_F}c_1wr_3^2(\theta)d\theta\\ &=\frac{c_1wr_{OI}^2}{2\tan\varphi_1}\left\{-\exp\left[2(\theta_I-\theta_F)\tan\varphi_1\right]+1\right\} \end{aligned} \tag{30}$$

The overall energy dissipation rate of the instability body is

$$D=D_{AF}+D_{BI}+D_{IF} \tag{31}$$

In accordance with the upper-bound principle of limit analysis method, the exterior force power in the instability body equals the interior energy dissipation rate.

$$-W_{SP}+W_r+W_u=D_{AF}+D_{BI}+D_{IF} \tag{32}$$

Substituting Eqs. (13), (14), (27), (28), (29), and (30) into Eq. (31), the limit supporting force on underwater shield tunnel face in soft-hard heterogeneous strata considering seepage can be obtained as

$$\sigma_{sp}=rDN_r+r_wN_u+\sigma_{u'}-cN_c \tag{33}$$

Where, N_r, N_u, and N_c represent the dimensionless stability coefficients of soil weight, pore water seepage, and soil cohesion, respectively.

The restriction conditions of Eq. (33) are $0<\theta_B<\theta_I<\theta_A<\frac{\pi}{2}$, $\theta_A<\theta_F<\pi$ and $r_{OA}<r_{OB}$. $\sigma_{sp\max}$ is solved by MATLAB traversal grid algorithm.

3. Stability analysis of tunnel face in soft-hard uneven strata

3.1 Determination of stability analysis method

3.1.1 Numerical modeling and calculation parameters

An underwater shield tunnel model is set up by FLAC3D finite difference software. A section of the underwater shield tunnel crosses the soft-hard heterogeneous strata. The upper stratum of the tunnel is mainly muddy clay, and the lower stratum is limestone soil. The property parameters of upper-soft and lower hard-strata are presented in Table 1. The outer diameter of the single circular underwater shield tunnel is 14.5 m, and the inner diameter is 13.3 m. The lining ring is comprised of segments, the segment width is 2 m, and its

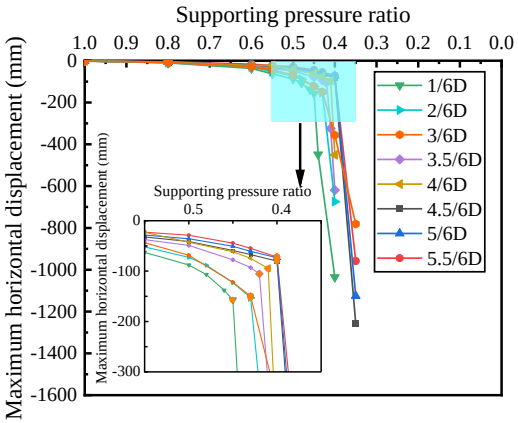

Fig. 2 Maximum horizontal displacement and supporting pressure ratio

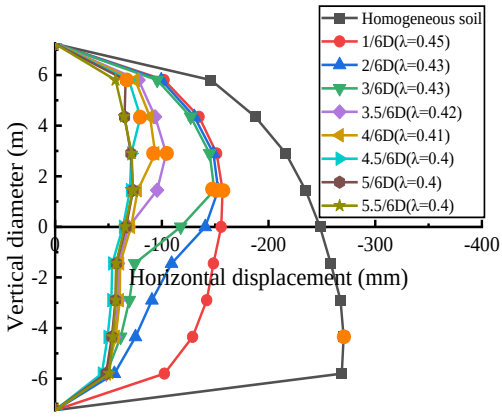

Fig. 3 Horizontal displacement

thickness is 0.6 m. The elastic modulus of the lining is 3.06×10^{10} Pa. The grouting layer thickness is 0.2 m. According to the practical project, the tunnel burial depth is 20 m, and the water depth is 12 m. Owing to the symmetry of the tunnel structure, the overall dimension of the model is 65.45 m×100 m×78.2 m. The soil around the tunnel and the grouting layer adopt eight-node hexahedral elements, shell elements are selected for the lining, and link elements are used to simulate the interaction of the lining with the surrounding soil masses. The boundary conditions are set as follows: the upper surface of the model is a free boundary, the horizontal displacements of the left and right sides and front and rear sides of the model, and the vertical displacement of the bottom are all restricted. The left and right sides and front and rear sides of the model, and the bottom are impermeable boundaries. In the fluid-solid coupling calculation, 120 kPa pore water pressure and 120 kPa vertical force act on the upper surface of the model. Only 120 kPa vertical force acts on the upper surface of the model when the seepage effect is not considered.

3.1.2 Determination of limit supporting pressure of tunnel face

When the interface between the soft-hard heterogeneous strata is located at different positions of the excavation face, the relation curves of the supporting pressure ratios and the maximum horizontal displacements of the excavation face considering fluid-solid coupling are presented in Fig. 2. Based on the mutation criterion of the stability principle, the mutation points of the curves under different ratios are obtained, and the supporting pressure ratios under different working conditions are determined referring to the distribution of the plastic region in the soil accounting fluid-solid coupling, as shown in Table 2. Fig. 3 presents the horizontal displacements of the vertical tunnel diameter accounting the fluid-solid coupling as the excavation face loses stability under different thickness ratios of upper-soft and lower-hard strata and homogeneous soil stratum. The results reveal that with decreasing the thickness of the soft soil layer in the excavation face, the horizontal displacement of the vertical diameter gradually decreases, and the location of the maximum horizontal displacement gradually transfers from lower to upper part of the excavation face. When the thicknesses of the hard soil layer are 2/6*D*, 3/6*D*, 3.5/6*D*, 4/6*D*, and 4.5/6*D*, respectively, the instability first occurs in the soft soil layer, then the excavation face loses stability, which demonstrates the local instability of the soft soil layer results in the global face instability.

Table 2 Limit supporting pressures under different interfaces

Interface thickness ratio	Limit supporting pressure ratio	Limit supporting pressure (kPa)	Maximum horizontal displacement when instability (mm)
1/6*D*	0.45	265.350	-156.95
2/6*D*	0.43	253.556	-152.89
3/6*D*	0.43	253.556	-149.19
3.5/6*D*	0.42	247.660	-104.15
4/6*D*	0.41	241.763	-93.83
4.5/6*D*	0.4	235.866	-79.96
5/6*D*	0.4	235.866	-73.04
5.5/6*D*	0.4	235.866	-72.84
Homogeneous soft soil stratum	0.48	283.039	-279

Table 2 shows the limit supporting pressure ratios and the maximum horizontal displacements under different thicknesses of the hard soil layer and homogeneous soft soil stratum when considering fluid-solid coupling. We can conclude that the limit supporting pressure ratio of the shield tunnel face gradually reduces with increasing the thickness of the hard soil layer in the range of the excavation face as the excavation face loses stability, and the limit supporting pressure, and the maximum horizontal displacement are also gradually reduced. The reason is that the cohesion and the internal friction angle of the hard soil layer are larger than those of the upper soft soil layer, hence, the hard soil layer has relatively high strength and strong self-stability. With the increase of the thickness of the hard soil layer, the local stability of the excavation face enhances, resulting in the decrease of the limit supporting pressure and the maximum horizontal displacement as the face loses stability, which is similar to the results reported by Senent and Jimenez (2015), and Wang (2017).

Referring to the limit supporting pressures and the maximum horizontal displacements under homogeneous soft

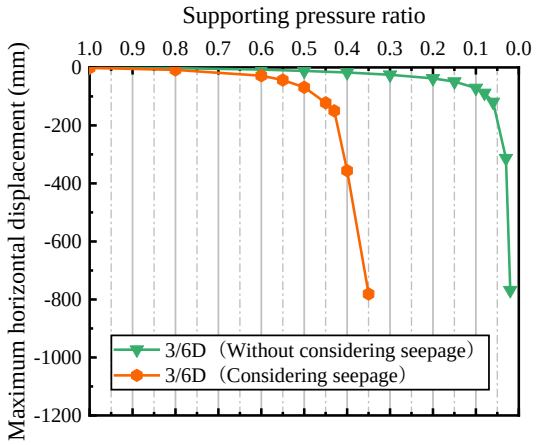

Fig. 4 Maximum horizontal displacement and supporting pressure ratio

soil stratum and different thickness ratios of the hard soil layer, it is proposed that during the large-diameter shield tunneling in the soft-hard heterogeneous strata, when the thickness of the hard soil layer within the excavation face is less than 1/6*D*, the limit supporting pressure of the excavation face can be calculated on the basis of the uniform distribution of the soft soil layer in the whole section. When the thickness of the hard soil layer is more than 1/6*D*, the interface of the soft-hard soil layer can be placed at the tunnel axis.

3.2 Verification of limit supporting pressure under multi-stratum seepage

3.2.1 Limit supporting pressure considering and without considering seepage

When the interface of the upper-soft and lower-hard strata is located at the tunnel axis, Fig. 4 shows the relation curves of the supporting pressure ratios and the maximum horizontal displacements of the excavation face considering and without considering seepage. On the basis of the sudden change of the maximum horizontal displacement, the limit supporting pressure ratio of the excavation face is 0.43 when taking the fluid-solid coupling effect into account, and the corresponding limit supporting pressure is 253.566 kPa. As the seepage effect is not accounted, the limit supporting pressure ratio is 0.06, and the corresponding limit supporting pressure is 29.941 kPa. It is indicated that the effect of the seepage force is the major component of the total limit supporting pressure on the underwater shield tunnel face in the soft-hard heterogeneous strata, and the effect of seepage cannot be ignored in the face stability analysis of the underwater shield tunnel.

Accounting the seepage effect, the optimal solution of the part $rDN_r+r_wN_u\text{-}cN_c$ of Eq. (33) is 72.136 kPa by MATLAB programming. Fig. 5 presents the pore water pressure distribution in the soil when the excavation surface loses stability. From the figure, the pore water pressure distribution in the collapsed area is nearly even. The horizontal hydraulic gradient is primarily shown in the area before the face, and the vertical hydraulic gradient is basically presented in the area over the tunnel, which is consistent with the consideration of pore water pressure

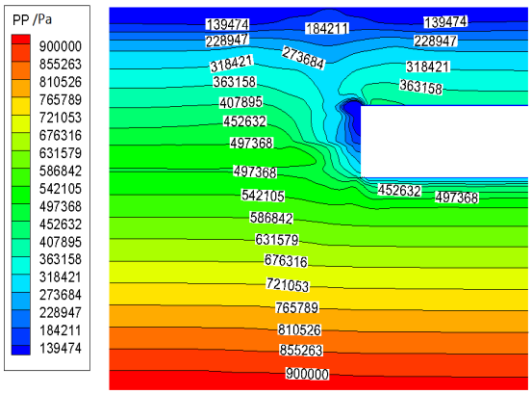

Fig. 5 Pore water pressure when the water level is 12 m

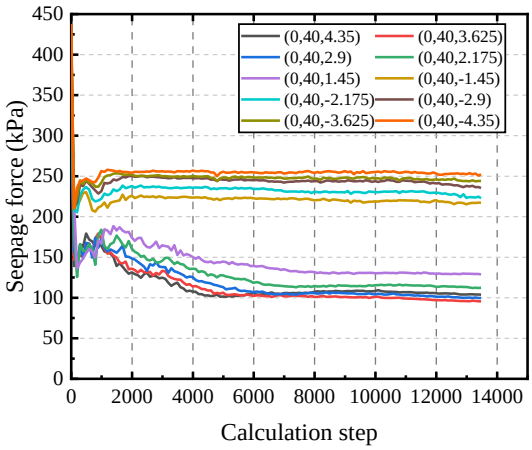

Fig. 6 The change of seepage force at feature points

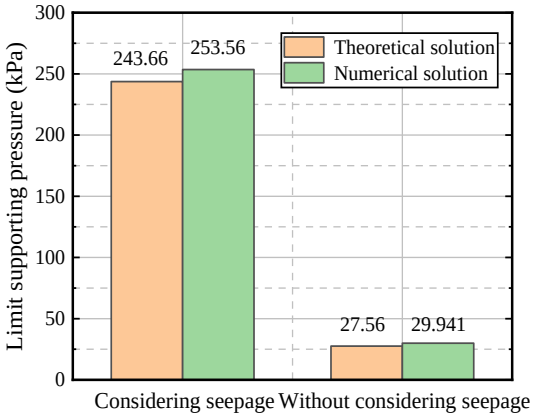

Fig. 7 Theoretical and numerical solutions of limit supporting pressure

distribution in the instability body in Section 2.2. Fig. 6 presents the changes of pore water pressure at some feature points on the excavation face during the numerical analysis. The seepage force σ_u on the excavation face under steady seepage is 171.526 kPa according to the method proposed in Section 2.2. Then, the total limit supporting pressure is 243.662 kPa. Using the theoretical method under multi-stratum reported in Section 2, the theoretical solutions of the limit supporting pressure on the excavation face

Table 3 Property parameters of the soil

	Natural weight (N/m^3)	E (Pa)	μ	φ(°)	c (Pa)	Permeability coefficient (m/s)
Silt(1)	16.5×10^3	7.88×10^6	0.3	18.93	14.05×10^3	1×10^{-8}
Silt(2)	16.8×10^3	8.36×10^6	0.3	19.11	14.38×10^3	1×10^{-8}
Silt clay	17.5×10^3	10×10^6	0.3	20	14×10^3	1×10^{-8}
limestone	23.4×10^3	200×10^6	0.21	40	20×10^3	1×10^{-10}

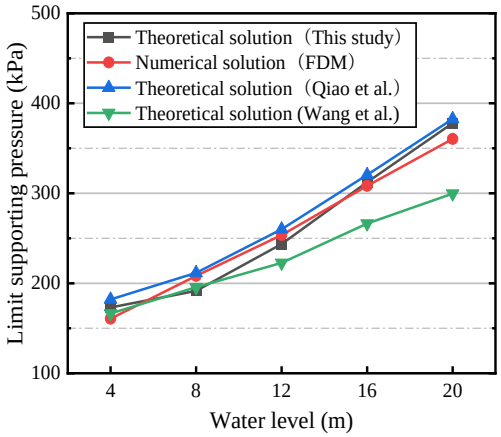

Fig. 8 Theoretical and numerical solutions of limit supporting pressure

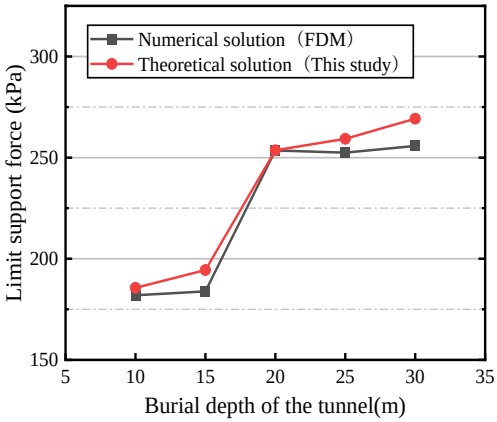

Fig. 9 Theoretical and numerical solutions of limit supporting pressure

accounting and without accounting seepage are obtained. Fig. 7 presents that the numerical solutions of the limit supporting pressure are close to the theoretical solutions under the two conditions, which demonstrates the correctness of the instability model of the underwater shield tunnel face and the reliability of the calculation method of the limit supporting pressure in the present study.

3.2.2 Validity of the logarithmic spiral model

Using the limit equilibrium analysis, Qiao *et al*. (2010) established a wedge model considering seepage, and explored the face stability of the multi-stratum shield tunnel. Employing the limit upper-bound analysis, Wang *et al.* (2013) proposed a three-block instability model of tunnel face to analyze the limit supporting pressure under seepage. The theoretical solutions and the numerical solutions of the limit supporting pressure accounting multi-stratum seepage of this study are compared with the theoretical solutions of the three-dimensional wedge model(Qiao *et al*. 2010) and the three-block instability model(Wang *et al.* 2013), as presented in Fig. 8. We can obtain that as the water level rises, the limit supporting pressures of the three-block instability model are smaller than those of the other three methods. When considering seepage in the upper-soft and lower-hard strata, the theoretical solutions and the numerical solutions of the limit supporting pressure obtained in this study are close to each other under different water levels. As the water level rises, the variation laws of the two are relatively consistent with that of the theoretical solutions of the three-dimensional wedge model. Since the calculation principle of Qiao *et al*.'s method is different from the other two, the theoretical solutions of the limit supporting pressure of the wedge model are slightly larger than that of the logarithmic spiral model, and the numerical solutions under each water level.

The reason is that in the wedge model considering seepage proposed by Qiao *et al.* (2010), the shape of loose soil above the sliding wedge block is a prism when the excavation face loses stability, and it has fully developed to the riverbed surface. More soil and pore water does work on the excavation face, so the theoretical solutions of the limit supporting pressure analyzed by Qiao *et al.* (2010) are larger. For the limit upper-bound approach and numerical analysis approach in this study, the reduction of the disturbed soil range caused by the soil stress transfer, and the soil arching effect in the upper soil above the tunnel are considered, which is consistent with the conclusions obtained by Liu *et al*. (2021): When the tunnel burial depth is large, the overlying strata include a sliding development zone and a stable arching zone. Therefore, the limit supporting pressures obtained by these two methods are small.

The theoretical solutions and the numerical solutions of the limit supporting pressure accounting seepage are shown in Fig. 9 when the tunnel burial depths under multi-stratum conditions are 10 m, 15 m, 20 m, 25 m, and 30 m, respectively. We can obtain that when the seepage effect is considered, the change laws of the theoretical solutions and the numerical solutions of the limit supporting pressure of the multi-stratum underwater shield tunnel are similar, and the values of the two are close to each other. When the burial depth is larger than 20 m, the change of theoretical solution tends to be gentle because of the soil arching effect above the tunnel.

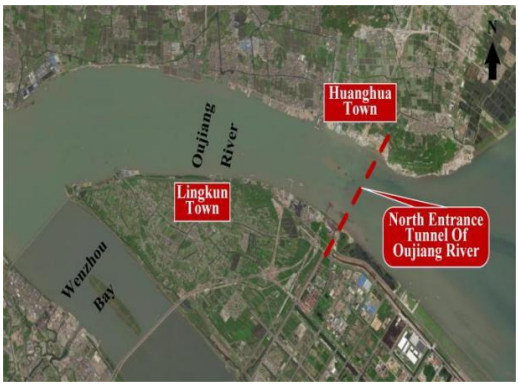

Fig. 10 Project location diagram

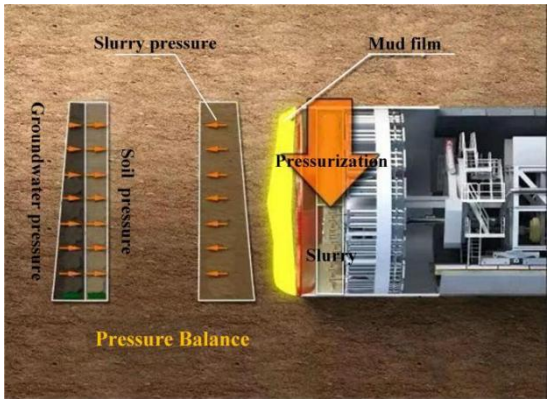

Fig. 11 Working principle diagrammatic drawing of the shield

To sum up, the above analysis validates the reliability of the theoretical calculation method and numerical simulation method of the limit supporting pressure accounting seepage in the upper-soft and lower-hard strata in the present study.

4. Engineering example analysis

In the first stage project of the line S2 of Wenzhou municipal railway, the Oujiang Beikou Tunnel project is located at the estuary of the Oujiang River. It goes down across the waters of the Oujiang Beikou, and advances northward to Huanghua Town. The project location is presented in Fig. 10. The typical soil layer distribution of the project is presented in Table 3. The underwater shield tunnel with a diameter of 14.9 m is excavated by a mud balanced shield, Fig. 11 shows the working principle diagrammatic drawing of a mud balanced shield. Other parameters of the shield tunnel structure are shown in Section 3. The project is located in a strong tidal sea area. The water depth varies from 4 m to 20 m. In the middle of the shield section below the Oujiang River, the shield crosses the upper-soft and lower-hard strata.

4.1 Influence of water level on tunnel face stability

Relied on the actual project, the tunnel burial depth 20 m, and the water levels are 4 m, 8 m, 12 m, 16 m, and 20 m, respectively. The shield tunnel face stability in the soft-hard heterogeneous strata accounting seepage is investigated.

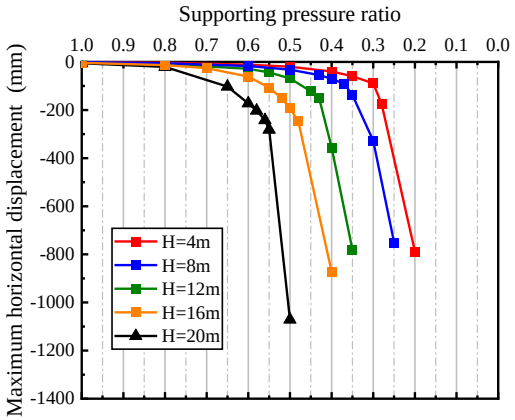

Fig. 12 Maximum horizontal displacement and supporting pressure ratio

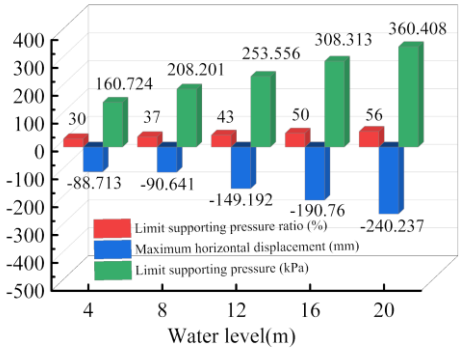

Fig. 13 Limit supporting pressure and maximum horizontal displacement

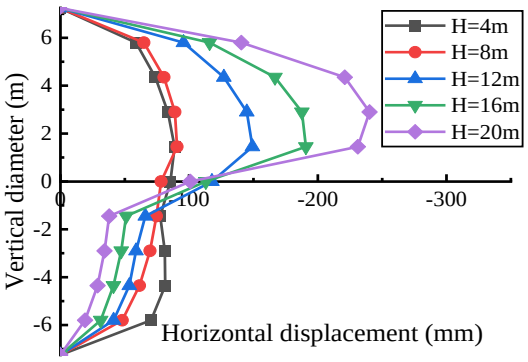

Fig. 14 Horizontal displacement

4.1.1 Tunnel face deformation

Fig. 12 presents the relation curves between the supporting pressure ratios and the maximum horizontal displacements of the excavation face in the soft-hard heterogeneous strata as the water level changes. On the basis of the mutation criterion of stability principle, Fig. 13. presents the limit supporting pressure and the maximum horizontal displacement under the corresponding water level. From the figure, the limit supporting pressure ratio and the limit supporting pressure increase linearly as the the water level rises in upper-soft and lower-hard strata. When the excavation face loses stability,

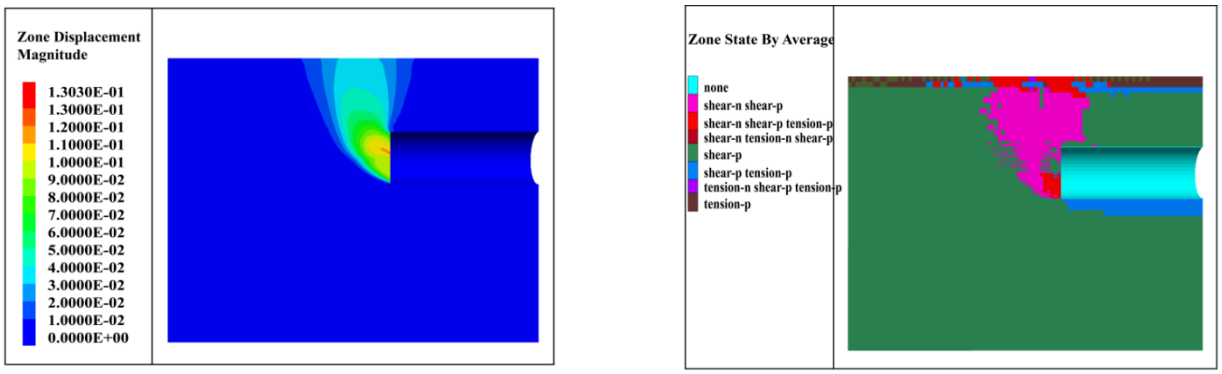

(a) H=4 m

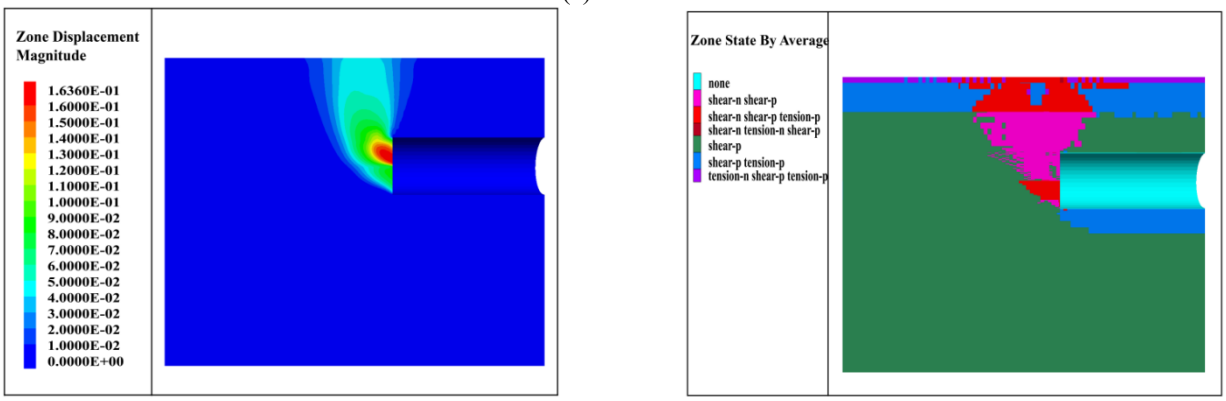

(b) H=12 m

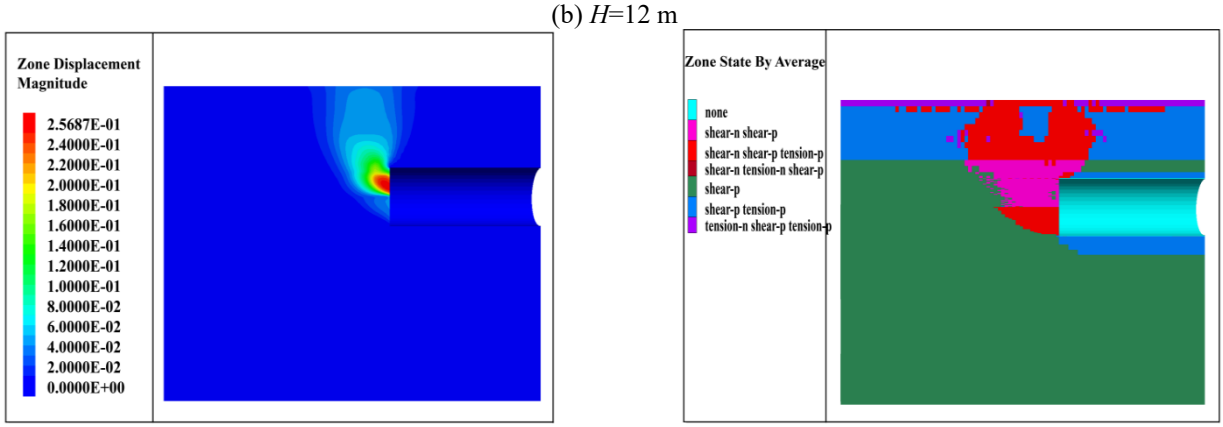

(c) H=20 m

Fig. 15 Displacement and plastic region

from Fig. 14, we can obtain that the maximum horizontal displacement appears in the soft soil layer of the excavation face, and it increases as the water level rises. The results demonstrate that the seepage significantly affects the face stability of underwater tunnels. The conclusions are consistent with those obtained by Wang *et al.* (2013), Zou and Qian(2018) and Li *et al.* (2021): Seepage significantly affects the tunnel face stability during tunneling. The total supporting pressure increases linearly with the rising water table as accounting the seepage. The reason is that the higher water table enlarges the hydraulic gradient before the tunnel face, so the larger seepage force enhances the limit supporting pressure. Thus, accounting the effect of the tide, the mud pressure and the excavation parameters should be regulated timely with the water level fluctuation. Meanwhile, the amount of synchronous grouting should be increased, and the water stop ring and secondary grouting should be conducted timely.

4.1.2 Tunnel face stability mode

The total displacement and the plastic region distribution are shown in Fig. 15 when the water levels are 4 m, 12 m, and 20 m, respectively, when the tunnel face loses stability in the soft-hard heterogeneous strata. Accounting the fluid-solid coupling action, the instability first takes place in the upper soft soil layer. When the water level is low, the water head gradient around the excavation face is small, and the effect of seepage force upon the excavation face stability is little. A sizeable spiral area before the face slips into the slurry pressure tank when the instability occurs. With the water level rise, the impact of the seepage force on the stability of the upper soft soil layer is becoming more and more obvious. When the water level

is 20 m, the excavation face instability mainly occurs in the soft soil layer under high water pressure seepage. According to the plastic region distribution under different water levels, the plastic region develops upward to the riverbed surface when the excavation surface loses stability, and the plastic region is in a funnel-shape. The higher water level enlarges the plastic region in the upper part above the tunnel, and the plastic region fully develops.

4.2 Influence of burial depth on tunnel face stability

The water depth is 12 m. When the burial depths of the shield tunnel are 10 m, 15 m, 20 m, 25 m, and 30 m, respectively, the limit supporting pressure and the failure mode of the underwater tunnel face in upper-soft and lower-hard strata under fluid-solid coupling are analyzed.

4.2.1 Excavation face deformation

In the soft-hard heterogeneous strata, under different burial depths the relation curves of the supporting pressure ratios and the maximum horizontal displacements of the excavation face are presented in Fig. 16. The limit supporting pressure ratio is determined in combination with the distribution of the plastic region in the soil accounting fluid-solid coupling.

From Fig. 17, when the excavation face loses stability, the maximum horizontal displacements take place at the upper part of the excavation face under different burial depths. When the burial depth is shallow, the horizontal displacement of the soft soil layer within the excavation face is larger than that of the hard soil layer. As the burial depth increases, the horizontal displacement of the lower part of the excavation face increases gradually, however, it is still less than the maximum horizontal displacement of the excavation face. It is demonstrated that the face instability of the underwater shield tunnel in the soft-hard heterogeneous strata under fluid-solid coupling is the global face instability induced by the local instability in the soft soil layer. When the burial depth is shallow ($C \leq 15$ m), the horizontal displacement of the upper part of the excavation face increases gradually. However, when the burial depth increases ($C \geq 20$ m), the horizontal displacement of the upper part of the excavation face reduces because of the soil arching effect.

Fig. 18 shows that when the burial depth of the shield tunnel gradually increases from 10 m to 20 m, the limit supporting pressure of the excavation face gradually increases. The limit supporting pressure of the shield tunnel face changes little when the burial depth increases from 20 m to 30 m. The reason is that the soil arching effect gradually formed in the upper soil layer above the excavation face with increasing the tunnel burial depth, and the water-soil pressure above the soil arch cannot be transmitted to the excavation face, which does not affect the excavation face stability. The works done by the vertical earth pressure and seepage force below soil arch are approximate. Thus, limit supporting pressure changes little.

4.2.2 Excavation face failure mode

Fig. 19 presents the total displacement and the plastic region distribution when the burial depths are 10 m, and 30 m, respectively, as the face instability occurs in the soft-hard heterogeneous strata. When the burial depth is 20 m, the distributions of the displacement and the plastic region are the same as those of 12 m water level, as presented in Fig. 15(b). Accounting the fluid-solid coupling effect, the excavation face instability first takes place in the upper soft soil layer under different burial depths. As the depth of the tunnel is shallow(C=10 m), the excavation face instability mainly occurs in the upper soft soil layer, and it has little effect on the deformation of the lower hard soil layer. The settlement of the soil before the excavation face can develop upward to the

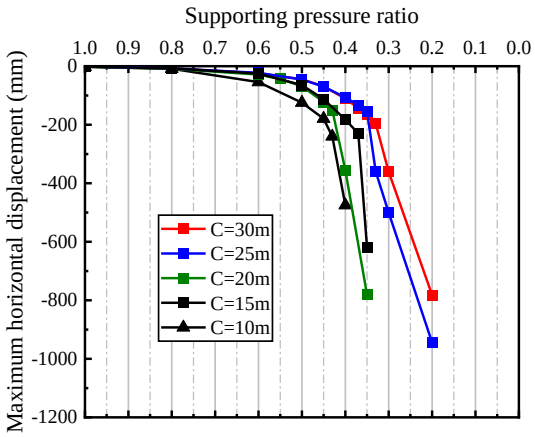

Fig. 16 Maximum horizontal displacement and supporting pressure ratio

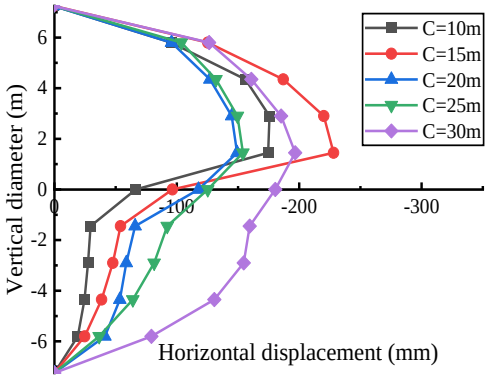

Fig. 17 Horizontal displacement of vertical diameter

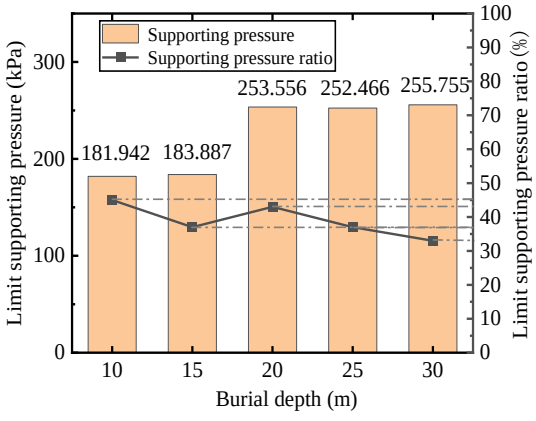

Fig. 18 Limit supporting pressure

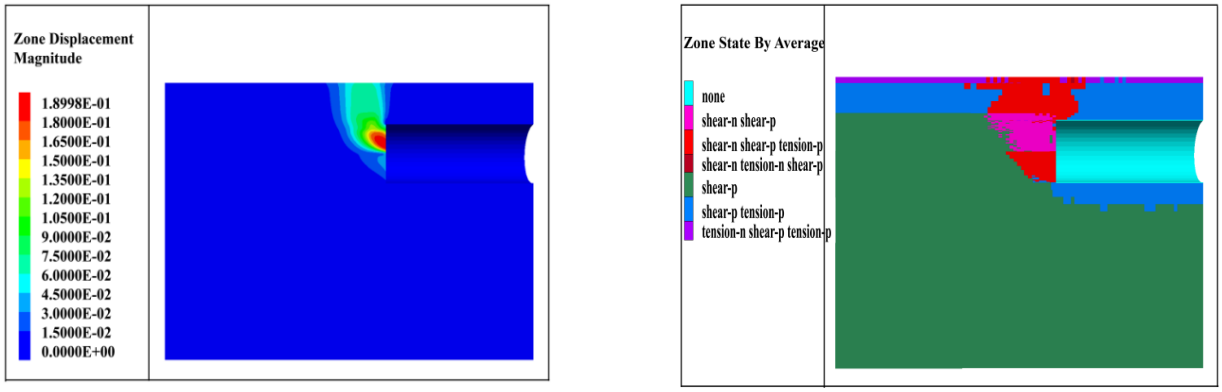

(a) C=4 m

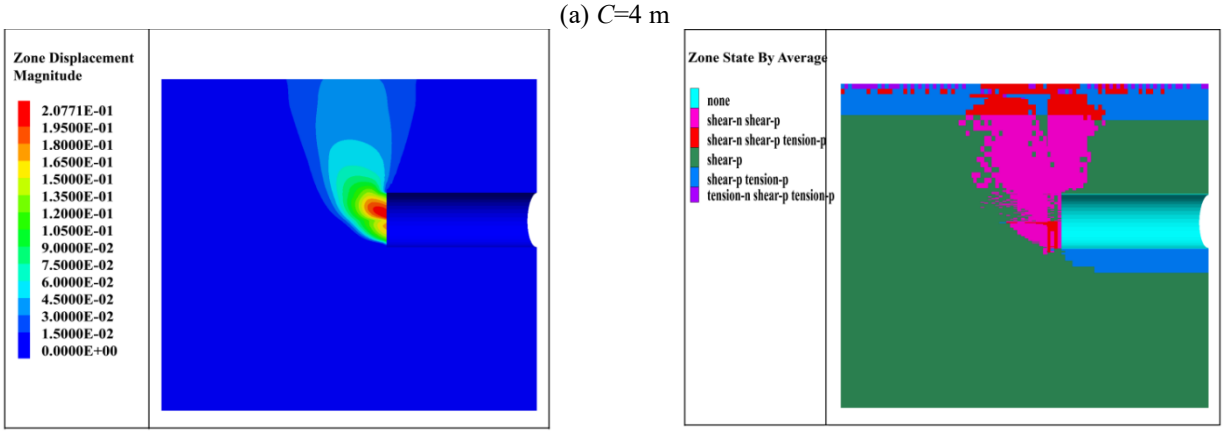

(b) H=30 m

Fig. 19 Displacement and plastic region

riverbed sufficiently. With the increase of the burial depth, the instability of the soft soil layer leads to the increase of the displacement of the lower hard soil layer. Owing to the soil arching effect, the settlement of the soil develops upward insufficiently. Deeper burial depth(C=30 m) makes the law more obvious. With the increase of tunnel burial depth, the plastic region before the excavation face enlarges, but the upward development is insufficient.

5. Conclusions

- A logarithmic spiral instability model of a large-diameter underwater shield tunnel face considering seepage in soft-hard uneven strata is proposed. The effect of high water pressure seepage upon the face stability of the underwater tunnel can be regarded as the seepage force upon the excavation face, and the pore water seepage force in the instability body. In the instability body, the vertical seepage effect is mainly considered in the soil above the excavation face, and the horizontal seepage effect is primarily considered in the soil in front of the excavation face. The correctness and reliability of the analytical solution of the limit supporting pressure are validated by numerical method and literature methods.
- In the stability analysis of large-diameter underwater shield tunnel face in upper-soft and lower-hard strata, when the thickness of the hard soil layer within the excavation face is less than 1/6D, the limit supporting pressure can be calculated according to the uniform distribution of soft soil in the whole face. When the thickness of the hard soil layer exceeds 1/6D, the interface of the soft and hard soil layer can be placed at the axis of the tunnel to calculate the limit supporting pressure.
- The effect of the seepage force is the major component of the total limit supporting pressure of underwater shield tunnel face in upper-soft and lower-hard strata. The effect of seepage cannot be ignored in the face stability analysis of the underwater shield tunnel.
- The limit supporting pressure ratio and the limit supporting pressure increase linearly in upper-soft and lower-hard strata with rising the water level. The higher water level enlarges the horizontal displacement of the upper soft soil layer due to the seepage force. The plastic region fully develops in the upper part above the tunnel as the water level rises.
- Under different burial depths, the instability of the underwater shield tunnel face in upper-soft and lower-hard strata first occurs in the upper soft soil layer. Due to the soil arching effect, with the increase of burial depth, the horizontal displacement of the upper part of the excavation face decreases, and the limit supporting pressures of the excavation face are relatively close; the plastic region before the excavation face enlarges, but the upward development is insufficient.

Acknowledgments

This work was supported by the National Natural Science Foundation of China (Grant No. 52178389), and the Science and Technology Planning Project of Zhejiang Traffic Quality Supervision Industry (Grant No. ZJ201906).

References

Anagnostou, G. (2012), "The contribution of horizontal arching to tunnel face stability", *Geotechnik*, **35**(1), 34-44. https://doi.org/10.1002/gete.201100024.

Anagnostou, G. and Kovári, K. (1996), "Face stability conditions with earth-pressure-balanced shields", *Tunn. Undergr. Sp. Tech*., **11**(2), 165-173. https://doi.org/10.1016/0886-7798 (96)00017 -X.

Alagha, A.S.N. and Chapman, D.N. (2019), "Numerical modelling of tunnel face stability in homogeneous and layered soft ground", *Tunn. Undergr. Sp. Tech*., **94**(11), 1-14. https://doi.org/10.1016/j.tust.2019.103096.

Ahmed, M. and Iskander, M. (2012), "Evaluation of tunnel face stability by transparent soil models", *Tunn. Undergr. Sp. Tech*., **27**(1), 101-110. https://doi.org/10.1016/ j.tust.2011.08.001.

Broere, W. (2001), "Tunnel face stability & new CPT applications", Ph. D. Dissertation; Delft University of Technology, Delft, Netherlands.

Broms, B.B. and Bennermark, H. (1967), "Stability of clay at vertical openings", *J. Soil Mech. Found Div*., **93**(1),71-94.

Chen, R.P., Lin, X.T. and Wu, H.N. (2019), "An analytical model to predict the limit support pressure on a deep shield tunnel face", *Comput. Geotech*., **115**, 1-11. https://doi.org/ 10.1016/ j.compgeo.2019.103174.

Cheng, X.S., Li, G.L., Chen, J., Zhang, K. and Du, X.L. (2018), "Seismic response of a submarine tunnel under the action of a sea wave", *Mar. Struct*., **60**, 122-135. https://doi.org/ 10.1016/j.marstruc.2018.03.004.

Cheng, X.S., Zhang, S.L., Qi, L. and Zhou, X. H. (2021), "Fluid-solid coupling response of shield tunnel lining structure under high water pressure", *Mar. Georesour. Geotec*., https://doi.org/10.1080/1064119X.2021.1971805.

Chen, R.P., Tang, L.J., Ling, D.S. and Chen, Y.M. (2011), "Face stability analysis of shallow shield tunnels in dry sandy ground using the discrete element method", *Comput. Geotech*., **38**(2), 187-195. https://doi.org/10.1016/j.compgeo.2010. 11.003.

Chen, R.P., Li, J., Kong, L.G. and Tang, L.J. (2013), "Experimental study on face instability of shield tunnel in sand", *Tunn. Undergr. Sp. Tech*., **33**, 12-21. https://doi.org/ 10.1016/j.tust.2012.08.001.

Chen, R.P., Yin, X.S., Tang, L.J. and Chen, Y.M. (2018), "Centrifugal model tests on face failure of earth pressure balance shield induced by steady state seepage in saturated sandy silt ground", *Tunn. Undergr. Sp. Tech*., **81**, 315-325. https://doi.org/10.1016/j.tust.2018.06.031.

Davis, E.H., Gunn, M.J., Mair, R.J. and Seneviratine, H.N. (1980), "The stability of shallow tunnels and underground openings in cohesive material", *Géotechnique*, **30**(4), 397-416. https://doi.org/10.1680/geot.1980.30.4.397.

Horn, N. (1961), "Horizontal earth pressure on the vertical surfaces of the tunnel tubes", *Proceedings of the National Conference of the Hungarian Civil Engineering Industry*, Budapest, November. 7-16. (In German).

Hu, X.Y., Zhang, Z.X. and Kieffer, S. (2012), "A real-life stability model for a large shield-driven tunnel in heterogeneous soft soils", *Front. Struct. Civ. Eng*., **6**, 176-187. https://doi.org/10.1007/s11709-012-0149-7.

Han, K.H., Zhan, C.P. and Zhang, D.L. (2016), "Upper-bound solutions for the face stability of a shield tunnel in multilayered cohesive-frictional soils", *Comput. Geotech*., **79**(10), 1-9. https://doi.org/10.1016/j.compgeo.2016.05.018.

Hu, X.Y. and Zhang, Z.X. (2013), "Research on particle flow approach for modeling face failure mechanism in slurry shield tunneling under complex ground conditions", *Chin. J. Rock Mech. Eng*., **32**(11), 2258-2267.

Ibrahim, E., Soubra, A.H., Mollon, G., Raphael, W., Dias, D. and Reda. A. (2015), "Three-dimensional face stability analysis of pressurized tunnels driven in a multilayered purely frictional medium", *Tunn. Undergr. Sp. Tech*., **49**(6), 18-34. https://doi.org/10.1016/j.tust.2015.04.001.

Idinger, G., Aklik, P., Wu, W. and Borja, R.I. (2011), "Centrifuge model test on the face stability of shallow tunnel", *Acta Geotech*., **6**(2), 105-117. https://doi.org/10.1007/ s11440-011-0139-2.

Jancsecz, S. and Steiner, W. (1994), "Face support for a large mix-shield in Heterogeneous ground conditions", Symposium Tunnelling' 94. London:Chapman and Hall Limited, 531-550.

Leca, E. and Dormieux, L. (1990), "Upper and lower bound solutions for the face stability of shallow circular tunnels in frictional material", *Géotechnique*., **40**(4), 581-606. https://doi.org/10.1680/geot.1 990.40.4.581.

Lee, I.M., Nam, S.W. and Alm, J.H. (2003), "Effect of seepage forces on tunnel face stability", *Can. Geotech. J*., **40**(2), 342-350. https://doi.org/10.1139/t02-120.

Lei, H.Y., Zhang, Y.J., Hu, Y. and Liu, Y.N. (2021), "Model test and discrete element method simulation of shield tunneling face stability in transparent clay", *Front. Struct. Civ. Eng*., **15**, 147-166. https://doi.org/10.1007/s11709-020-0704-6.

Lv, X.L., Zhou, Y.C. and Li, F.D. (2016), "Centrifuge model test and numerical simulation of stability of excavation face of shield tunnel in silty sand", *Rock Soil Mech*., **37**(11), 3324-3328+3335. https://doi.org/10.16285/j.rsm.2016.11.035.

Lu, P., Yuan, D.J., Chen, J., Jin, D.L., Wu, J. and Luo, W.P. (2021), "Face stability analysis of slurry shield tunnels in rock-soil interface mixed ground", *KSCE J. Civ. Eng*., **25**(6), 2250-2260. https://doi.org/10.1007/s12205-021-1254-8.

Liu, K.Q., Dias, D., Ding, W.T. and Chen, R. (2021), "Influence of soil-arching effect on tunnel face stability", *Int. J. Geomech*., **21**(7), 04021107. https://doi.org/10.1061/(ASCE)GM.1943-5622.0002060.

Li, W., Zhang, C.P., Tan, Z.B. and Ma, M.S. (2021), "Effect of the seepage flow on the face stability of a shield tunnel", *Tunn. Undergr. Sp. Tech*., **112**(2021), 103900. https://doi.org/10.1016/j.tust.2021.103900.

Mollon, G., Dias, D. and Soubra, A.H. (2010), "Face stability analysis of circular tunnels driven by a pressurized shield", *J. Geotech. Geoenviron. Eng*., **136**(1), 215-229. https://doi.org/10.1061/(ASCE)GT.1943 -5606.0000194.

Mollon, G., Dias, D. and Soubra, A.H. (2011), "Rotational failure mechanisms for the face stability analysis of tunnels driven by a pressurized shield", *Int. J. Numer. Anal. Met*., **35**(12), 1363-1388. https://doi.org/10.1002/nag.962.

Perazzelli, P., Leone, T. and Anagnostou, G. (2014), "Tunnel face stability under seepage flow conditions", *Tunn. Undergr. Sp. Tech*., **43**, 459-469. https://doi.org/10.1016/j.tust.2014.03.001.

Qiao, J.L., Zhang, Y.T. and Gao, J. (2010), "Stability analysis of shield tunnel face in multilayer soil with seepage", *Rock Soil Mech*., **31**(5), 1497-1502. https://doi.org/10.3969/ j.issn. 1000-7598.2010.05.025.

Senent, S. and Jimenez, R. (2015), "A tunnel face failure mechanism for layered ground, considering the possibility of partial collapse", *Tunn. Undergr. Sp. Tech*., **47**, 182-192. https://doi.org/10.1016/j.tust.2014.12.014.

Tang, X.W., Liu, W., Albers, B. and Savidis, S. (2013), "Upper bound analysis of tunnel face stability in layered soils", *Acta Geotech*., https://doi.org/10.1007/s11440-013-0256-1.

Ukritchon, B., Yingchaloenkitkhajorn, K. and Keawsawasvong, S. (2017), "Three-dimensional undrained tunnel face stability in clay

with a linearly increasing shear strength with depth", *Comput. Geotech*., **88**, 146-151. https://doi.org/10.1016/j.compgeo.2017.03.013.

Wang, J., Lin, G.J., Xu, G.W., Wei,Y.Q., Li, S.Q., Tang, X. and He, C. (2021), "Face stability of EPB shield tunnels in multilayered ground with soft sand lying on hard rock considering dynamic excavation process: A DEM study", *Tunn. Undergr. Sp. Tech*., **120**, 1-15. https://doi.org/10.1016/j.tust.2021.104268.

Wang, H.R., Huang, M.S., Lv, X.L. and Zhou, W.X. (2013), "Upper-bound limit analysis of stability of shield tunnel face considering seepage", *Chin. J. Geotech. Eng*., **35**(9), 1697-1704.

Wang, J. (2017), "Study on the disturbance induced by EPB shield tunneling in mixed ground with soft sand lying on hard rock", Ph.D. Dissertation; Xinan Jiaotong University, Chengdu, China (in Chinese).

Xue, Y.G., Li, X., Qiu, D.H., Ma, X.M., Kong, F.M., Qu, C.Q. and Zhao, Y. (2019), "Stability evaluation for the excavation face of shield tunnel across the Yangtze River by multi-factor analysis", *Geomech. Eng*., **19**(3), 283-293. https://doi.org/10.12989/gae.2019.19.3.283.

Zhong, J.H. and Yang, X.L. (2020), "Kinematic stability of tunnel face in nonuniform soils", *KSCE J. Civ. Eng*., **24**(2), 670-681. https://doi.org/10.1007/s12205-020-0996-z.

Zou, J.F. and Qian, Z.H. (2018), "Face-stability analysis of tunnels excavated below groundwater considering coupled flow deformation", *Int. J. Geomech*., **18**(8), 04018089. https://doi.org/10.1061/(ASCE)GM.1943-5622.0001199.

Zhang, C.P., Li, W., Zhu, W.J. and Tan, Z.B. (2020), "Face stability analysis of a shallow horseshoe-shaped shield tunnel in clay with a linearly increasing shear strength with depth", *Tunn. Undergr. Sp. Tech*., **97**, 103291. https://doi.org/ 10.1016/j.tust.2020.103291.

Zhang, S.L., Cheng, X.S. Qi, L. and Zhou, X.H. (2022), "Face stability analysis of large diameter shield tunnel in soft clay considering high water pressure seepage", *Ocean Eng*., https://doi.org/1 0.1016/j.oceaneng.2022.111283.